1 **Comparison of debris-flow observations, including fine sediment grain size and**
2 **composition, and runout model results at the Illgraben, Swiss Alps**
3
4

5 [1,2]Daniel Bolliger, [1]Fritz Schlunegger[*], [3]Brian W. McArdell
6
7 [1]Institute of Geological Sciences, University of Bern, Switzerland
8 [2]Geotest AG, Zollikofen, Switzerland
9 [3]Swiss Federal Institute WSL, Switzerland
10 *Corresponding author: fritz.schlunegger@unibe.ch
11
12

13 **Abstract**

14 Debris flows are important processes for the assessment of natural hazards due to their
15 damage potential. To assess the impact of a potential debris flow, parameters such as the
16 flow velocity, flow depth, maximum discharge and the volume are of great importance. This
17 study uses data from the Illgraben observation station, Central Alps of Switzerland, to explore
18 the relationships between these flow parameters and the debris flow dynamics. To this end,
19 we simulated previous debris flow events with the RAMMS debris flow runout model, which is
20 based on a numerical solution of the shallow water equations for granular flows using the
21 Voellmy friction relation. Here, the events were modeled in an effort to explore possible
22 controls on the friction parameters μ and ξ, which describe the Coulomb friction and the
23 turbulent friction, respectively, in the model. Additionally, sediment samples from levee
24 deposits were analyzed for their grain size distributions (14 events) and their mineralogical
25 properties (four events) to explore if the properties of the fine-grained matrix have an influence
26 on the debris flow dynamics. Finally, field data from various debris flows such as the flow
27 velocities and depths were statistically compared with the grain size distributions, the
28 mineralogical properties, and the simulation results to identify the key variables controlling the
29 kinematics of these flows. The simulation results point to several ideal solutions, which depend
30 on the Coulomb and turbulent friction parameters (μ and ξ, respectively). In addition, the
31 modelling results show that the Coulomb and turbulent frictions of a flow are related to the
32 Froude number if the flow velocity is < 6-7 m/s. It is also shown that the fine-sediment grain
33 size or clay-particle mineralogy of a flow neither correlates with the flow's velocity and depth,
34 nor can it be used to quantify the friction in the Voellmy friction relation. This suggests that the
35 frictional behavior of a flow may be controlled by other properties such as the friction generated
36 by the partially fluidized coarse granular sediment. Yet, the flow properties are well-correlated

37   with the flow volume, from which most other parameters can be derived, consistent with

38   common engineering practice.

1   Introduction

1.1   Debris flows, and parameters controlling their velocity and runout

Debris flows are rapid mass movements consisting of water-saturated and poorly sorted debris with a large range of grain sizes. Debris flows tend to develop one single or a suite of multiple surges with steep coarse-grained fronts. Their motion is driven by gravity and resisted by friction within the flow and at the boundary with the channel bed (Iverson, 1997). The boulder-rich front is then followed by a tapering body where the pore fluid pressures are large, often exceeding the hydrostatic pressure (Iverson, 1997, McArdell et al., 2007). In the frontal part, larger particles tend to ascend in the debris flow body due to particle collisional stresses thereby building a coarse-grained top layer (Johnson et al., 2012), which travels somewhat faster than the flow front itself, delivering coarse sediment to the front. Accordingly, the coarser-grained particles along with some of the fine sediment present at the surface of the flow tend to accumulate in the surge head and are deposited laterally in levees just a few meters behind the front (Johnson et al., 2012).

In the past years, de Haas et al. (2015) conducted experiments to investigate how the grain size distribution and water content influences the velocity of a debris flow. They found that a higher clay content tends to result in an increase of both the velocity and the runout distance of such flows. However, if the clay content becomes too large, then the velocity decreases due to a higher viscosity of the fluid. This relationship should also be applicable to the silt fraction because clay and silt particles are a part of the fluid while grains larger than silt contribute to the solids of a debris flow (Iverson, 1997). The experiments of de Haas et al. (2015) also showed that a large gravel content in the flow front leads to a strong frictional resistance, which in turn reduces the flow velocity. In addition, a large gravel content results in a larger pore water diffusivity, which reduces the pore pressure in the flow and contributes to a further reduction of the flow velocity. On the other hand, a low gravel content leads to lower collisional forces, which might also lead to a relatively low flow velocity. Furthermore, also according to the experiments by de Haas et al. (2015), the water content, the velocity, the volume, and the runout distance of a debris flow are positively correlated to each other. Based on a combination of experimental and field data, Hürlimann et al. (2015) came to the same conclusions, and they additionally found that an increase in the clay content generally leads to a reduction in the runout distance. Indeed, the absorption of water in swelling clay minerals has the potential to result in an increase of the cohesion of a flow, which in turn could cause a reduction of the flow velocity and the runout distance. Finally, using laboratory experiments, Kaitna et al. (2016) documented that a relatively high fraction of fine-grained material tends to occur in flows with excess pore fluid pressures. In addition, these authors mentioned that such flows were characterized by low fluctuations of normalized fluid pressures and normal stresses, and the experiments showed that the shear stresses were concentrated

3

76 at the base of the flow. Based on the conclusions of the aforementioned authors, we expect
77 to see a dependency of the flow properties in the Illgraben and the granulometric composition
78 of these flows (Uchida et al., 2012), and we anticipate that the flow velocity is negatively
79 correlated with the relative abundance of the finest-grained particles.

80 The mineralogical composition of a flow is a further parameter, which has the potential to
81 impact the rheology and thus the flow velocity and runout distance of debris flows, yet these
82 relationships have largely been overlooked in the literature. In particular, because clay
83 minerals are important constituents of the fine-grained fraction of these flows, they have the
84 potential to regulate the pore fluid pressure and the stress state through their ability to absorb
85 water in their crystal structure (Di Maio et al., 2004). This is mainly the case for swelling clay
86 minerals (see also section above) such as those of the smectite group (Di Maio et al., 2004),
87 where the pore fluid composition has a large influence on the volume and the shear strength
88 of these minerals (Chatterji and Morgestern, 1990; Di Maio, 1996). Because shear stresses
89 within a flow are a direct consequence of the friction between the particles and the fluid phase
90 and since the friction properties directly influence the propagation of a debris flow (see section
91 1.2), we anticipate the occurrence of a direct relationship between the velocity and runout
92 distance of debris flows, and the mineralogical composition of the fine-grained matrix.

93

94 *1.2   Physically-based models describing debris flow processes, and goal of paper*

95 There are several rheological models or flow resistance relationships describing the behavior
96 of debris flows such as the flows' velocities, runout distances and frictional properties (e.g.,
97 Allen, 1997; Rickenmann, 1999; Naef et al., 2006). One commonly used approach is the
98 Voellmy friction relation (Voellmy, 1955; Salm, 1990; 1993; Christen et al., 2012), which is
99 also implemented in the software RAMMS, a software package to simulate debris flow runout
100 (see section 3.1). In the Voellmy friction equation, the frictional resistance of a flow S [Pa] is
101 composed of the sum of two friction terms: (i) A dry Coulomb-type friction term, referred to as
102 Coulomb friction, describes the frictional resistance between the debris flow and the channel
103 bed and mainly depends on the flow depth; and (ii) a drag or viscous-turbulent friction term
104 describes the turbulent frictional resistance, which mainly depends on the dynamic pressure
105 and thus on the velocity of the flow. Both components are characterized by the coefficients μ
106 and ξ, which control the values of the Coulomb and the turbulent frictions, respectively
107 (Christen et al., 2012). Optionally, cohesion stresses can be included in an extended Voellmy
108 friction equation (Bartelt et al., 2015; Berger et al., 2016). Because this additional cohesion
109 term has rarely been used in engineering practice and is apparently relatively small (Berger
110 et al., 2016), it was neglected herein, and the friction equation takes the following form:

111 $S = \mu N + \dfrac{\rho g v^2}{\zeta}, N = \rho g h \cdot \cos{(\varphi)}$ *(1),*

112   where S is the frictional resistance [Pa], ρ the density of the debris flow, h the flow height (or

113   flow depth), g the gravitational acceleration, φ the slope angle of the channel bed, and v the

114   velocity of the flow.

115   A simplified approach to characterize a debris flow is the Froude number, which describes the

116   ratio between the inertial and the gravitational forces:

117    $Fr = \frac{v}{\sqrt{gh}}$ (2),

118   where Fr is the Froude number, v the velocity of the flow, g the gravitational acceleration and

119   h the flow height (Hübl et al., 2009; Choi et al., 2015).

120   As mentioned above, the velocity and runout distance of debris flows are likely to depend on

121   the frictional resistance in such mass movements. This friction, in turn, can be characterized

122   by two coefficients μ and ξ in the Voellmy friction relation (1). Because we anticipate that the

123   mineralogical and granulometric composition of the fine-grained matrix has an influence on

124   the properties of such flows (see section 1.1), we expect to identify a relationship between the

125   frictional properties of a flow, its velocity, and its grain size and mineralogical composition.

126   Here, we test and explore these hypotheses using in-situ data collected at the Illgraben debris

127   flow monitoring station situated in the Central European Alps (Figure 1), and we evaluate the

128   data with the results of a numerical runout model referred to as RAMMS. Upon combining field

129   data with modelling results, we aim at identifying those parameters that have the largest

130   control on the dynamic properties of the debris flows at the Illgraben.

131

132   **2   Study site and setting**

133   The Illgraben catchment is located in the Valais region in western Switzerland (Figure 1). It

134   extends from the summit of the Illhorn (2716 m asl) to the outlet of the Illgraben into the Rhone

135   River (610 m asl). The total area of about 9.5 km^2 consists of the Illgraben basin, which has a

136   spatial extent of 4.6 km^2, and the Illbach tributary catchment covering 4.9 km^2 (Figure 1a). The

137   Illgraben basin has been very active and has generated several debris flows each year

138   (Schlunegger et al., 2009; McArdell and Satori, 2022). The rates of sediment discharge in the

139   Illgraben have been exceptionally high for Alpine standards (Berger et al., 2011a). Several

140   studies showed that the erosion rates and the numbers and extents of debris flows strongly

141   depend on the hydro-climatic parameters such as the average annual temperature and the

142   precipitation rates (Bennett et al., 2013; Hirschberg et al., 2019; 2021a, b).The highly fractured

143   bedrock (Bumann, 2022), belonging to the Penninic nappe stack (Gabus et al., 2008), consists

144   of massive-bedded limestones, quartzites and Triassic schists with dolobreccia interbeds.

145   Schlunegger et al. (2009) considered these lithologies to be the main source of the silt and

146   clay fraction that constitute the matrix of the debris flow deposits. Based on a petrographic

147   analysis of the debris flow deposits, these authors also identified two distinct sediment sources

in the Illgraben where bedrock lithologies with different petrological properties are exposed. These are (i) a heavily fractured and foliated suite of gneisses and schists, which are exposed on the southern flank of the Illgraben, and (ii) a vertically plunging succession of limestones, dolomites and cellular dolomites, which make up the northwestern flank of the Illgraben (Figure 1). The material from these two sources is very well mixed in response to repeated deposition and remobilization of sediment within the catchment (Schlunegger et al., 2009). The sediment cascade has been subject to seasonal variations, where smaller debris flows events are associated with net sediment accumulation in the channel, while large flows can entrain sediment up to several times their initial mass along their flow paths (Berger et al., 2010; Berger et al., 2011a, b; Schürch et al., 2011).

Grain size analyses conducted on samples from the channel bed and debris flow deposits indicated sand contents of 35-40% and clay contents of < 5% (Hürlimann et al., 2003; Schlunegger et al., 2009; Uchida et al., 2021). In the Rhone valley, an alluvial fan has formed covering an area of 6.6 km^2 (Schürch et al., 2016). The channel on the fan has a U-shaped cross-sectional geometry with a base that is about 5–10 m wide. For the lowermost 2 km, the gradient of the Illgraben channel ranges from about 7% to 18% (measured over a length of 50 m) with a mean of about 8% (Schlunegger et al., 2009). Thirty-one check dams with vertical drops of up to several meters were constructed along the lowermost 4.8 km of the channel to prevent the flows to further incise into the substratum (McArdell et al., 2007; Badoux et al., 2009). A debris flow monitoring station, situated on the lower fan c. 200 m upstream of the confluence with the Rhone River, was installed in 2000 and has been operated by the WSL since then (Hürlimann et al., 2003; Badoux et al., 2009). At the survey site (Figure 1c), the measured parameters include frontal velocity, flow depth, bulk density, maximum discharge rate, volumes, and normal and shear force (McArdell et al., 2007; McArdell, 2016). The related values are presented in the openly accessible database of the WSL (McArdell et al., 2023), and the data was collected using the methods presented in section 3.1. On average 3 to 5 debris flows have been registered by the measuring station every year. They have generally occurred during intense rainstorms between May and October (e.g., McArdell et al., 2007).

Figure 1
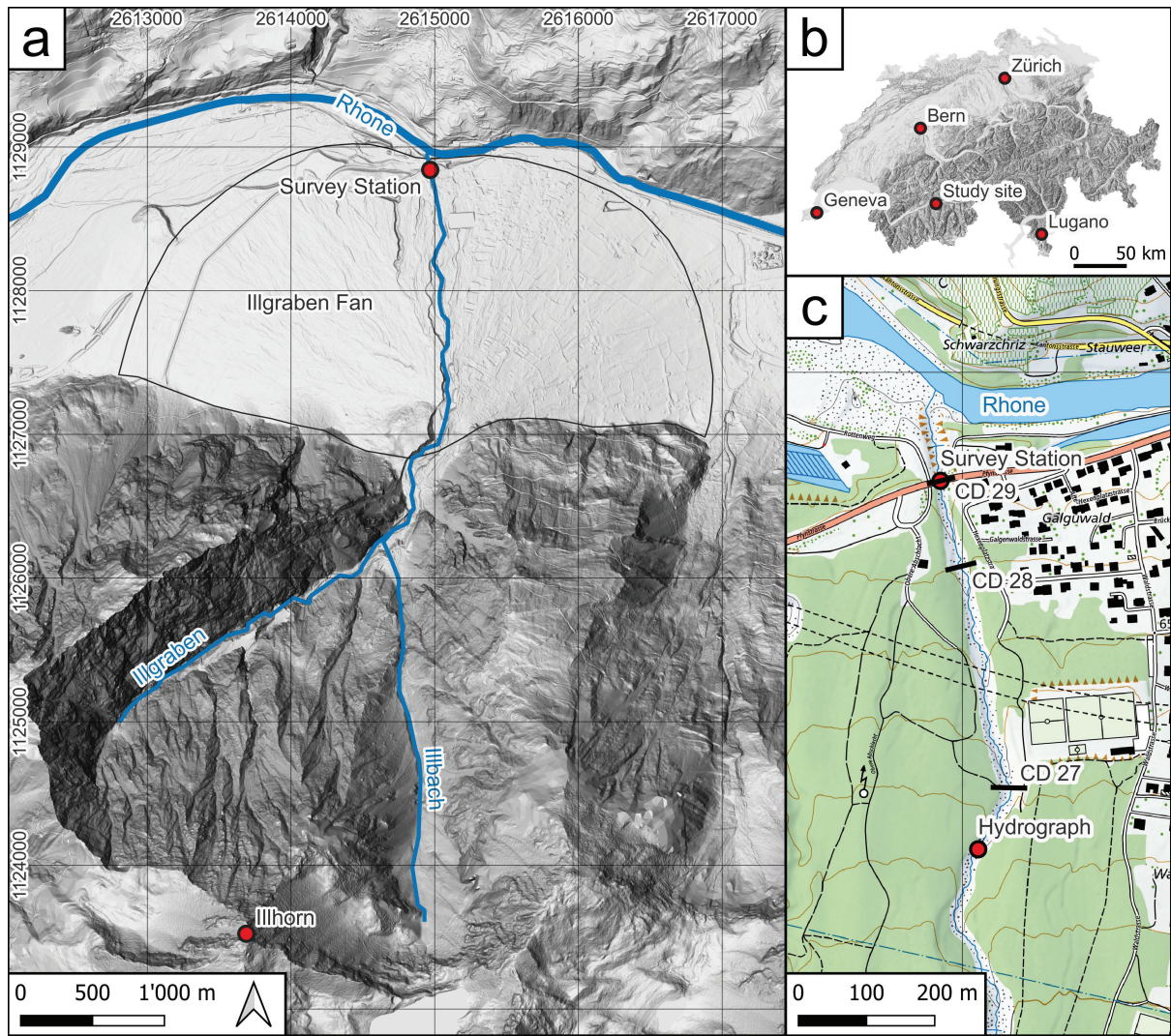
Figure 1: (a) Overview of the topographic situation around the Illgraben showing the Illgraben system with its river network consisting of the Illgraben, Illbach and the Rhone River. (b) Overview map of Switzerland with location of the study site. (c) Detailed topographic map of the Illgraben reach along which the RAMMS simulations have been conducted. It shows the location of the input hydrograph which was used as starting position for the modelling. The three check dams (CD) and the location of the survey station below the Pfynstrasse are displayed on this figure. The background is provided by the swissALTI3D and the Swiss Map Raster 10 (Swisstopo, 2022).

3   Methods

Using data collected in the field (section 3.1), we explored how the frictional properties of a debris flow influences the behavior (flow depth and velocity) of such a flow through modelling with RAMMS (section 3.2). We then tested whether the grain size distribution (section 3.3) and the mineralogical composition of the debris flow material (section 3.4) have an influence on the flow velocity.

192 *3.1   Surveys of debris flows*

193   Many of the in-situ measurements of the debris flow properties at the Illgraben have been

194   accomplished with a force plate that is installed in the channel beneath a bridge c. 200 m

195   upstream of the confluence with the Rhone River (survey station, see Figure 1c). At that survey

196   site, information on (i) the velocity, (ii) the flow depth, (ii) the mean bulk density, (iii) the

197   duration of individual debris flows, and (iv) the volumes of each flow have been determined in

198   the past years by the WSL (e.g., McArdell and Sartori, 2021; de Haas et al., 2022, Belli et al.,

199   2022; McArdell et al., 2023). As outlined in McArdell et al. (2007) and Schlunegger et al.

200   (2009), the force plate is a horizontal 8 m^2 steel structure, which is installed flush with the river

201   bed just on the top of the concrete check dam. The plate is equipped with normal and shear

202   force transducers. The flow depth is estimated using either a laser or radar unit. Because the

203   radar data is biased by an unpredictable smoothing of the flow surface, we preferentially used

204   the laser data for further calculations. Based on information about the flow depth and the

205   normal force, it was possible to determine the bulk density of a flow as it moves on the plate

206   itself. The volume of each flow was then calculated as the product between the velocity and

207   the cross-sectional area, and this product was integrated over the flow's duration (McArdell et

208   al., 2023). The frontal velocity is determined using the travel time of the flow front over the

209   reach upstream of the force plate (between check dams 27 or 28 and 29; Figure 1c and

210   Hürlimann et al., 2003). Table S1 presents a list of parameters, which been measured at the

211   Illgraben monitoring site, and Figure S1 displays screenshots from video recordings of

212   selected debris flows.

213

214   *3.2   Numerical modelling with RAMMS*

215   We explored, through modelling with RAMMS, how the frictional properties of a debris flow

216   influence its behavior such as flow depth and velocity. The RAMMS model was developed by

217   the Swiss Federal Institute for Forest, Snow and Landscape Research, WSL (WSL, 2022). It

218   is based on the two-parameter Voellmy-fluid model (Christen et al., 2012; Bartelt et al. 2015),

219   which describes the friction in the 2D depth-averaged equations of motion, which were

220   deviated for granular flows. We justify the selection of such an approach because in an

221   independent modelling study (FLATModel) calibrated with field data (Medina et al., 2007), the

222   Voellmy-fluid formula (eq. *1*) has been proven to reproduce the dynamics of debris flows (flow

223   velocity, erosion pattern in the channel, and aerial extension of the flow in the accumulation

224   zone) reasonably well. A major challenge for modelling is the choice of the input friction

225   coefficients. In particular, if the simulation cannot be calibrated with data that were collected

226   from a previous well-documented event (Christen et al., 2012; Deubelbeiss & Graf, 2011), the

227   input parameters have to be estimated. Because the model results such as the velocity, the

228   runout distance, and the flow depth are sensitive to the friction parameters μ and ξ (Bartelt et

229   al., 2015; Christen et al., 2012), we iteratively changed the values of these coefficients (Tables
230   S2 and S3) until we found, for each event, a best fit between the simulation results and the
231   observations.

232   The Coulomb friction coefficient μ is sometimes expressed as the tangent of the internal shear
233   angle (WSL, 2022). According to Salm (1993) an internal movement parallel to the slope is
234   only possible if the internal shear angle is smaller than the slope angle. Consequently, the
235   value of μ should be smaller than the tangent of the channel slope angle. For a minimum slope
236   angle of 7% (4°), μ should thus be smaller than 0.07. Therefore, for every debris flow event,
237   we conducted several simulations (between 12 and 43, Tabled S2 and S3) with μ varying from
238   0.01 to 0.06, and we modified the ξ parameter to minimize the z-value, which is explained with
239   eq. (*3*) below. This resulted in μ–ξ pairs with lowest z-values and thus best fits between the
240   model results and observations (such as the flow velocity v and the flow depth h). Please see
241   Tables S2 and S3 for information about the number of modelling runs, the intervals between
242   the μ– and ξ–values, and other input parameters that we used upon modelling.

243   We employed the 'hydrograph' input option of RAMMS to characterize the debris flows in the
244   model. Upon modelling, the hydrograph input was placed c. 500 m upstream of the survey site
245   (check dam 27, Figure 1c). Erosion was allowed to occur along the entire channel (Frank et
246   al., 2015; 2017) except at the check dams. Similar to the surveys in the field (section 3.1), the
247   model velocity was calculated using the travel time between check dams 28 and 29 (Figure
248   1c). The modelled flow depth values used herein were obtained as the average of the
249   measurements that were conducted at four points along a cross section at check dam 29.

250   The use of RAMMS requires a digital elevation model (DEM), event volume, and peak
251   discharge. The drone-based DEM, which is based on a survey conducted on the 10th of August
252   2021 (de Haas et al., 2022), was used for all simulations. However, this high-resolution DEM
253   did not cover the section of the channel between the Survey Station and the Rhone River
254   (Figure 1c). Therefore, in order to extend the area towards the confluence with the Rhone
255   River, the photogrammetry DEM, which has resolution of 0.1 m, was combined with an existing
256   0.5 m-lidar DEM (Swisstopo, 2022) using the software QGIS. Here, we resampled the drone-
257   based DEM to achieve the same resolution as the lidar DEM of Swisstopo (i.e., 0.5 m) so that
258   both datasets could be combined. The DEM of the short, concrete channel section beneath
259   the road bridge had to be reconstructed manually because it was not possible to image the
260   topography below the bridge. In addition, a filter (Serval-Raster editing tools, version 3.10.2)
261   was applied to the channel bed to smoothen the bed surface. This was done because a large
262   local change in the topography (such as a boulder) can induce strong vertical accelerations in
263   RAMMS (and other models that are based on the depth-averaged equations of motion), which
264   can lead to unrealistically large (or small) local flow depths.

265 Finally, we introduced a dimensionless *z*-value to describe the deviation of the simulated
266 velocity *v* and flow depth *h* from the measurements in the field:

267 $$z = \sqrt{\left(\frac{v_{simulation} - v_{measured}}{v_{measured}}\right)^2 + \left(\frac{h_{simulation} - h_{measured}}{h_{measured}}\right)^2} \qquad (3).$$

268 We thus explored how the model input parameters (μ– and ξ–values) affect the modelled
269 velocity and depth values of a flow. We then compared the model results with the surveyed
270 velocities and depths of each flow using eq. (*3*), which we implemented in the software Matlab
271 (R2021b).

272

273 *3.3 Grain size distribution*

274 For most of the debris flows that occurred in the years 2019, 2021 and 2022, at least one
275 sediment sample of 1.5 to 3 kg was taken from the levee deposits at the same site labelled as
276 'Survey Station' in Figure 1c (Swiss coordinates: 2'614'973, 1'128'842; Figure 1c). We
277 collected the material from underneath the bridge to prevent effects related to grain-size-
278 dependent erosion by rainfall. We selected the levee deposits for three reasons. First,
279 according to our experience, the levee deposits can better be attributed to a specific event
280 than other sediments of a debris flow. Second, the levee deposits are those sediments of a
281 debris flow that most clearly record the granulometric composition of the surge head, as our
282 observations on video recordings have shown. Third, it is the surge head, which exerts the
283 greatest control on the dynamics of a debris flow (McArdell et al., 2007; Johnson et al., 2012).
284 Accordingly, upon collecting material from levee deposits, we are likely to analyze sediments
285 with the highest potential to provide information that allows us to understand the dynamics
286 (e.g., flow depth and velocity) of past debris flows. Yet we acknowledge that this material is
287 more likely coarser grained than the sediments in the tail of such a flow (McArdell et al., 2007).
288 In the laboratory, all of the collected material was processed following the state-of-the-art
289 protocol (SN670 004–2b–NA norm), which was established at the Bern University of Applied
290 Sciences (Burgdorf). Following this protocol, the material was first dried and then sieved to a
291 minimum particle size of 0.5 mm using a set of 7 sieves, each of which has a defined mesh
292 size: 31.5 mm, 16 mm, 8 mm, 4 mm, 2 mm, 1 mm, and 0.5 mm. Subsequently, a slurry analysis
293 was carried out on the material < 0.5 mm using a hydrometer. The goal of this task was to
294 determine the particle size distribution between 0.1 and 0.001 mm. Finally, the grain size
295 distribution of the remining material between 0.5 and 0.063 mm was determined by wet
296 sieving. During this task, we used three sieves where the mesh size was 0.25 mm, 0.125 mm
297 and 0.063 mm. The grain size distribution was truncated at 16 mm so that the entire sample
298 is at least 100 times the mass of the largest particle (e.g., Church et al., 1987). We note,
299 however, that particles larger than 16 mm do occur on the levee deposits and we did sample
300 such material in the field. However, we were not able to consider this fraction due to technical

301 limitations in our laboratory and practical limitations on the mass of the sample necessary for
302 analysis.
303
304 *3.4 Powder XRD*
305 We hypothesize that clay minerals influence the pore pressure of a flow (Barshad, 1952),
306 which in turn could influence its mobility (McArdell et al., 2007). We expect such a control
307 because swelling clays tend to absorb water in their crystal structure. The result is an increase
308 in the viscosity of the flow, thereby reducing the dissipation of the fluid pore pressure. To test
309 this hypothesis, the mineralogical properties of some debris flow samples were measured
310 through standard powder XRD at the Institute of Geological Sciences of the University of Bern.
311 For this purpose, four samples were chosen from fast and slow velocity flows as well as from
312 deposits where either the coarse-grained or the fine-grained fractions dominate in the
313 analyzed grain size spectrum. To this end, the grain size fraction < 0.063 mm, which was
314 already extracted during the steps outlined above, was analyzed for powder XRD. Subsequent
315 milling with a vibrating-disc mill (Retsch RS 200) and a McCrone XRD-mill reduced the particle
316 sizes to the sub-micrometer scale. Corundum powder was added as standard to the samples,
317 and the samples were measured with the x-ray diffractometer X'Pert Pro MPD with Cu
318 radiation. Because this step did not include a determination of the mineralogic composition of
319 the clay minerals, a slightly different approach had to be employed. Here, we used the same
320 initial material, but it was only milled with the vibrating disc mill. The powder was then mixed
321 with a dispersant (0.1 molar NH_3) to achieve a homogeneous suspension. The clay particles
322 were separated in an Atterberg cylinder. The particles still in suspension after 15 hours were
323 extracted using a centrifuge. The extracted clay particles were then cleaned with HCl, $CaCl_2$
324 and deionized water. To distinguish between the different clay minerals, three sample holders
325 were either air dried, treated with ethylene glycol or heated to 400°C and 550°C before
326 measuring with the X'Pert Pro MPD with Cu radiation. The final processing of the data was
327 carried out with the software TOPAS (Coelho, 2018), which uses a Rietveld structure
328 refinement technique (Rietveld, 1969).
329
330 **4   Results**
331 *4.1   Survey results*
332 A total of 13 events from 2019, 2021, and 2022 were analyzed (Table S1, Table 1). The
333 measured flow velocities varied by one order of magnitude from 0.89 m/s to 8.69 m/s. The
334 maximum flow depths ranged from 1.13 m to 3.13 m, and the Froude numbers spanned the
335 interval between 0.27 to 2.35, pointing towards considerable differences in the dynamics of
336 these flows. The total volumes reached a maximum of c. 176,000 m^3 and the maximum

337 discharge rate was c. 190 m³/s. The measured density ranged from 1189 kg/m³ to 2323 kg/m³,

338 and the corresponding volumetric water contents were between c. 20% and 90%.

339

340 Table 1: Measured and analyzed debris flow events from 2019, 2021, and 2022. Velocity, flow depth, volume,
341 maximum discharge (Qmax) and density are the results of direct measurements at the monitoring station in the
342 Illgraben (Figure 1c). The Froude number was derived from these. The last two columns show, for which events
343 XRD analyses and RAMMS simulations were performed. The event of the 26th of July 2019 could not be simulated
344 due to the high Froude number.

Event date	Velocity [m/s]	Flow depth [m]	Froude number [ ]	Volume [m³]	Qmax [m³/s]	Density [kg/m³]	XRD analysis	RAMMS simulation
21.06.2019	6.62	3.13	1.19	97394	147.61	1870		✓
02.07.2019	3.86	1.75	0.93	73188	65.58	1971	✓	✓
26.07.2019	8.69	1.39	2.35	113310	93.26	2223	✓	
11.08.2019	6.95	1.81	1.65	88064	95.63	2323		✓
20.08.2019	0.89	1.13	0.27	6137	8.06	2031	✓	✓
24.06.2021	8.18	2.40	1.69	105032	162.20	1750		✓
06.07.2021	8.69	2.50	1.75	76906	186.61	1605		✓
16.07.2021	2.78	2.38	0.58	80879	60.70	1916	✓	✓
07.08.2021	2.32	2.49	0.47	38737	41.19	1884		✓
19.09.2021	1.25	1.13	0.38	8538	10.67	1697		✓
05.06.2022	3.39	2.08	0.75	39498	55.42	1690		✓
04.07.2022	8.18	2.49	1.66	175929	169.14	1189		✓
08.09.2022	1.91	1.93	0.44	9283	20.94	1592		✓

345

346 *4.2 Numerical modelling with RAMMS*

347 As mentioned above, we iteratively changed the μ– and ξ–friction values upon modelling until

348 we found a best-fit between the modelled and observed flow velocity and flow depth of each

349 flow (Tables S2 and S3). Because the latter properties of a debris flow (velocity and depth)

350 can be characterized by the Froude number (defined by eq. (2)), we first describe the

351 dependency of the modelled flow pattern on the Froude number, which itself is calculated

352 using the flow depth and velocity data of the field survey (Table 1). Please note that in this

353 context, eq. (2) predicts that changes in the flow velocity have a larger impact on the Froude

354 number than variations in flow depth. The simulations showed that RAMMS produces

355 reasonable results (e.g., Figure 2) for Froude numbers up to about 1.75 (Table 1). For larger

356 values (e.g., flows with large flow velocities), the simulations predict the occurrence of

357 standing waves at the debris flow front, which, however, have not been observed at the

358 Illgraben. Therefore, no simulations were possible for the event on the 26th of July 2019,

359 because this flow was characterized by a Froude number of 2.35. We acknowledge that roll-

360 waves, which could correspond to the standing waves simulated by RAMMS, do occur in a

361 debris flow, but such waves are mainly observed in the debris flow body and not at the
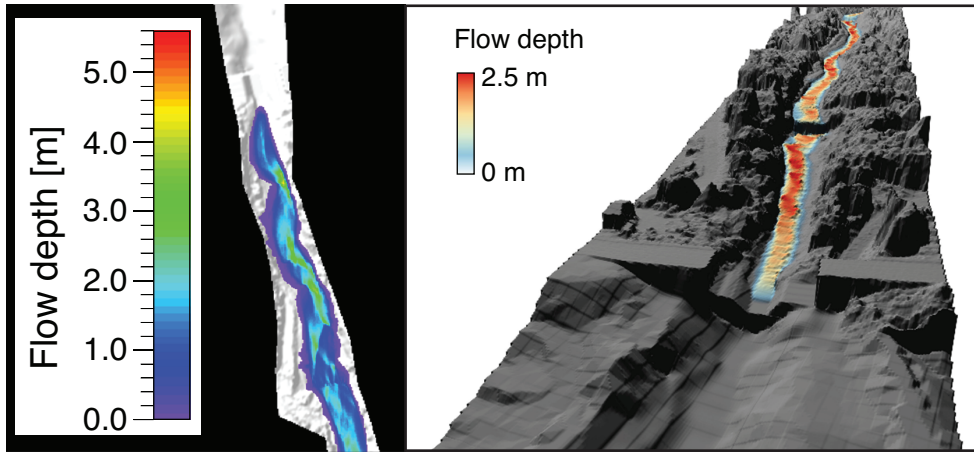
362 bouldery front.

363

Figure 2

Figure 2: Example of simulated flow depths. The image on the left shows flow depths in a 2D view provided by the RAMMS software. The image on the right shows a 3D view of the debris flow projected on a hillshade model using the QGIS software.
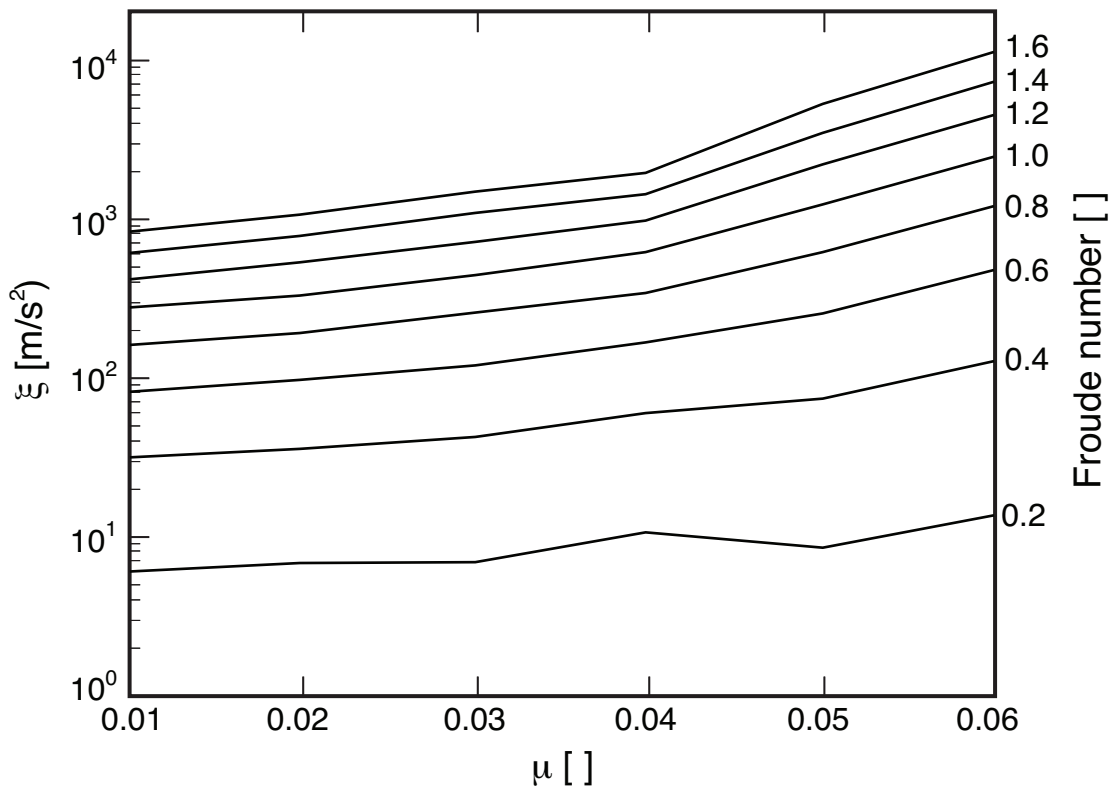

Figure 3

Figure 3: Modelled μ–ξ pairs, which result in a best fit between the observed and the modelled debris flow parameters. These latter values, in turn, appear to depend on the Froude numbers (based on measurements in the field, see Table 1) of the corresponding debris flow events.

The model results show that more than one best-fit μ–ξ pair is possible for successfully reproducing the observed velocity and depth of a flow (Table S4). Yet, on average, the lowest z-value is calculated for the μ–ξ pair with $\mu = 0.01$, followed by the pairs with $\mu = 0.02$ and $\mu =$

13

377 0.05. These values and patterns are consistent with the results of other debris flows analyses
378 conducted with RAMMS and applied to observations in e.g., the Alps (see Mikoš and Bezak,
379 2021, for an overview of related papers), the Himalayas near Luzhuang in China (Jianjun and
380 Zhang; μ– and ξ–values of 0.07 and 1500 m/s^2), and the coastal region in the vicinity of
381 Western Ghats in India (Abraham et al., 2021; μ– and ξ–values of 0.01 and 100 m/s^2,
382 respectively). In addition, Simoni et al. (2012) found that RAMMS successfully reproduced the
383 maximum observed runout distances of debris flows in the Italian Alps for μ–values close to
384 the energy gradient of the debris flow channel (which is the tangent of the surface slope). Our
385 modelling results support these inferences and additionally show that the modelled μ– and ξ–
386 relationships show a strong dependency on the corresponding Froude numbers calculated
387 from the field data (Figure 3, and Tables S4 and S5). Besides, for a given μ–value, the RAMMS
388 models predict that the ξ–values increase with the Froude number. Such an increase is more
389 obvious for large than for small μ–values (Figure 3, see also Table S5).

390

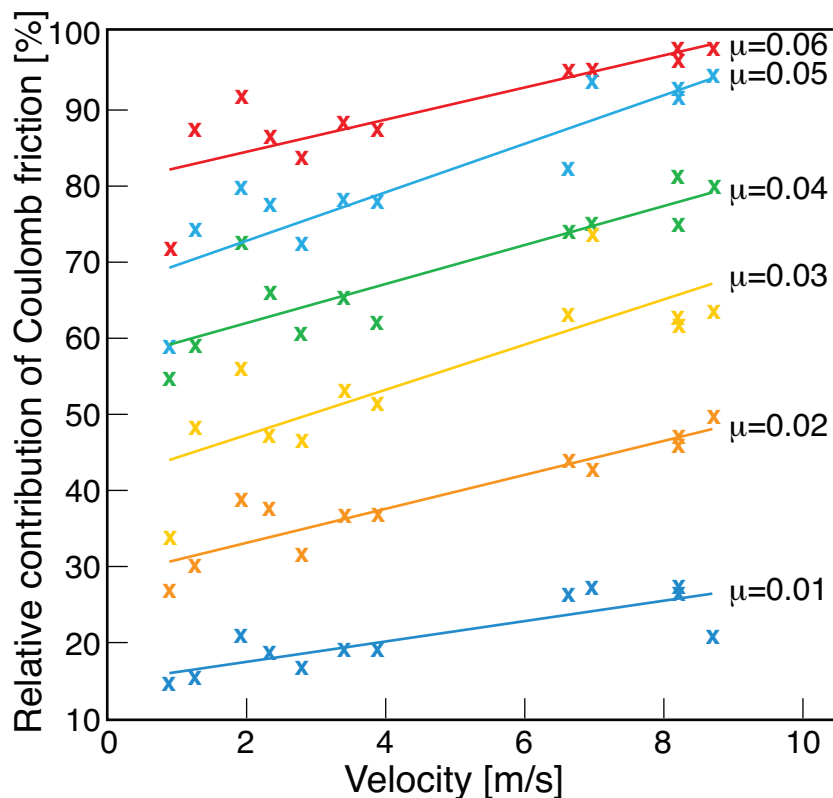391   Figure 4
392 Figure 4: Correlations between the relative contribution of the Coulomb friction to the total friction in
393 percent (y-axis) and the velocity of a debris flow (x-axis) for different μ-values. The data points refer to
394 best-fit simulations only. The lines are first order polynomial least square fitted trendlines.

395 Figure 4 illustrates that upon modelling, the relative contribution of the Coulomb friction to the
396 total friction increases with the flow velocity, and it shows that this contribution is greater for

14

397 large *μ*-values than for small ones. In particular, while the percentages of the Coulomb friction

398 are in the range of c. 20% for a *μ*-value of 0.01 and a flow velocity of < 1 m/s, they increase to

399 > 90% for a larger *μ*-value of 0.06 and a flow velocity of > 8 m/s.

400
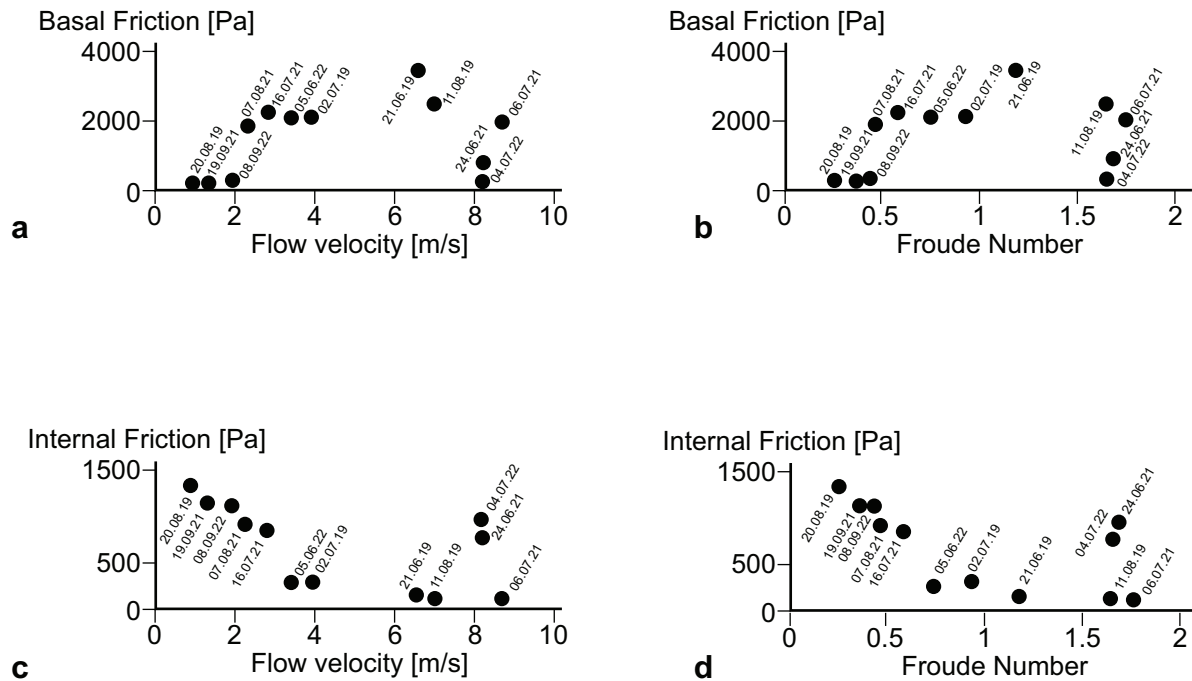
Figure 5

Figure 5: Relationships between a) flow velocity and Coulomb friction, b) Froude number and
Coulomb friction, c) flow velocity and turbulent friction, and d) Froude number and turbulent friction.
The plots show the results of the best-fit simulations for each flow.

404 The relationships elaborated above are further detailed in Figure 5, which documents the

405 dependency of the friction property (Coulomb and turbulent friction) of a flow on its velocity

406 and the corresponding Froude number. Note that for this analysis, we only considered the

407 results of the best-fit simulations of each flow. Accordingly, rapid debris flows with high Froude

408 numbers tend to be characterized by a large Coulomb friction, while slower debris flows are

409 simulated more reliably with a rather low Coulomb friction (Figures 5a, 5b). Conversely, flows

410 with a slow velocity tend to have a larger turbulent friction and are characterized by a low

411 Froude number, whereas the turbulent friction tends to be low for flows with a high velocity

412 and a high Froude number (Figures 5c, 5d). However, we note that the aforementioned

413 relationships between flow velocity, Froude number, turbulent and Coulomb friction break

414 down for flows that are more rapid than c. 6-7 m/s (Figure 5). Similar to the event on 26th of

415 July 2019, these flows are characterized by Froude numbers that are much larger than 1

416 (Table 1). These flows appear to be in a condition in which the relationships between friction

417 and flow properties are apparently non-linear and more complex than in flows, which can be

15

418 characterized by low Froude numbers. A further elaboration of this topic is, however, beyond

419 the scope of this paper.

420 Figure 6 summarizes the consequences of the aforementioned relationships. In particular,

421 small values of the Coulomb friction coefficient ($\mu \sim 0.01$), when the flow is moving on the

422 order of a few meters per second, indicate that the contribution of the Coulomb term to the

423 total friction is small, and that the total friction is therefore dominated by the turbulent friction

424 term (Figure 6). In the extreme case when $\mu = 0$, the turbulent friction term (eq. *1*) closely

425 resembles a Chezy friction from open-channel hydraulics (e.g. Henderson, 1966). Large

426 values of the Coulomb friction coefficient (here $\mu \sim 0.05$) suggest that the Coulomb friction

427 term is important, and that the contribution of the turbulent friction is correspondingly less

428 significant (Figure 6). Because we found ideal μ–ξ pairs with $\mu = 0.01$–0.02 and $\mu = 0.05$ for

429 most debris flows, we considered these flows to be dominated either by (i) the turbulent friction

430 (flows with $\mu = 0.01$–0.02) or by (ii) the Coulomb friction (flows with $\mu = 0.05$). Note that Figure

431 6 also shows that the total friction S increases with a larger μ. Nevertheless, the output of the

432 simulation (velocity and flow depth) is similar regardless of which μ–ξ pair variant is chosen.
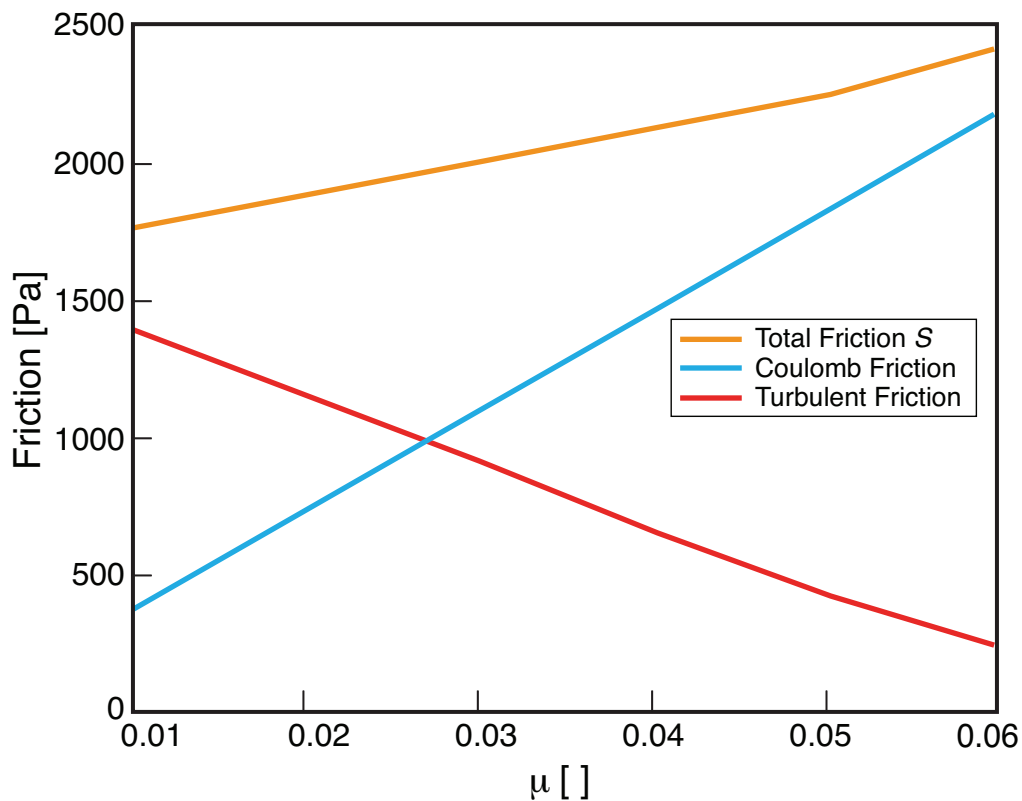
433

Figure 6

434

435 Figure 6: Values of Coulomb friction, turbulent friction, and total friction S as a function of the selected Coulomb
436 friction coefficient μ. The plotted values are averages of the friction magnitudes of all best-fit simulations. The blue
437 line represents the Coulomb friction contribution. The red line is the turbulent friction, and the yellow line is the total
438 friction.

439

4.3   Grain size distribution

Samples from 14 debris flows were analyzed for their grain size distribution (Figure 7 and Table S6). Note that there was a sediment sample but no monitoring data for the event on the 4th of October 2021. All events show a very similar grain size distribution. An exception, and thus an outlier, is a sediment sample that has a larger relative abundance of fine-grained material. This sample was taken from a debris flow, which occurred on the 2nd of July 2019. For all samples, the clay fraction has a relative mass abundance of 2–3%, the silt fraction 27–35%, the sand fraction 27–40% and the part of the gravel fraction that is covered by the analysis 23–37%. Note that the gravel fraction >16 mm was also analyzed (Table S6b). Yet we normalized the grain size data to 16 mm, because it was not feasible to collect larger mass-representative samples. Therefore, we acknowledge that the upper percentiles are affected and thus biased by this cut-off and the related percentage values have to be considered with caution.

For all samples, we measured grain sizes of 0.015–0.02 mm for the 16% percentile, 4–9 mm for the 84% percentile and 10–15 mm for the 95% percentile. The median grain size ranges from 0.15 mm to 0.5 mm. In general, the material was very poorly sorted with a skewness towards the fine-grained fraction. Interestingly, the grain size distribution was quite similar for all sampled material. Based on the available datasets, we are neither able to determine whether the mean grain size is more variable in space than in time, nor can we detect whether the coarse-grained fraction (>16 mm) could be highly variable whereas the fine-grained material is more homogeneous. However, similar to the mineralogical composition, which is also quite similar between the various flows, we interpret that the rather homogeneous granulometric composition at least of the fine-grained portion of the sediment is the direct consequence of the cascade of sediment mixing in the upstream part of the Illgraben (Schlunegger et al., 2009).
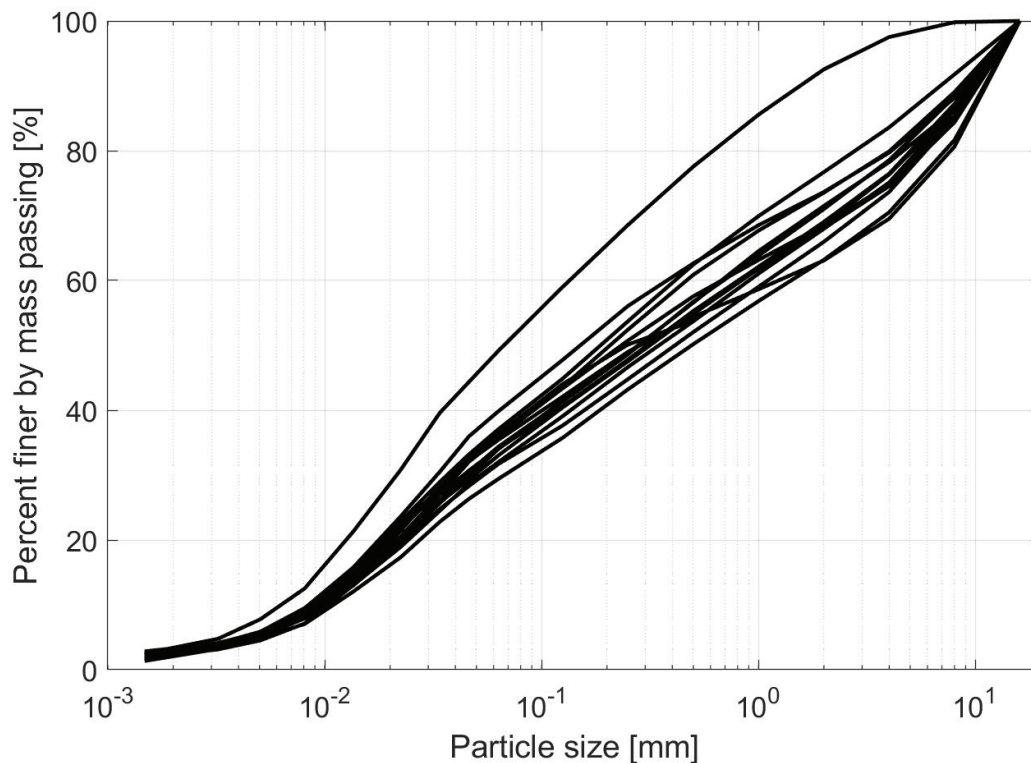
Figure 7

466

467 Figure 7: Diagram showing the grain size distribution of all 14 sampled debris flow deposits, truncated at a
468 maximum grain size of 16 mm.

469

470 *4.4 Powder XRD*

471 The results of the powder XRD analysis (Table S7) show that quartz was the main mineral of

472 the silt fraction and contributes between 29 and 36 wt% (Figure 8). In addition, dolomite (17–

473 24 wt%), muscovite (18–22 wt%), calcite (7–18 wt%) and illite minerals (8–12 wt%) are present

474 in all samples. Feldspar grains occur by < 5 wt%, and the clay minerals chlorite, kaolinite and

475 smectite are present in small quantities (< 1%) or are below the detection limit. Calcite shows

476 the greatest variation in the mineralogical composition with differences up to 11 wt%. The

477 other main components including quartz, dolomite, muscovite and illite show variations with a

478 maximum of 7 wt%. The feldspar minerals albite and orthoclase are very homogeneously

479 distributed in the four samples. Overall, the variations in the mineralogical composition

480 between the different samples are only minor and often lie within the methodological error of

481 ± 10% of the measured values. Yet, some albeit minor differences can be detected when the

482 compositions of the coarse- and fine-grained samples are compared. In the coarse-grained

483 sample, calcite crystals are more abundant than in the sample characterizing a fine-grained

484 debris flow. In contrast, the latter sample has a larger relative abundance of illite minerals than

485 the sample made up of coarser sediments. Although the database is sparse, we tentatively

18

486 consider these differences to reflect a source signal where the heavily fractured basement
487 rocks and Triassic schists, which also host the illite crystals, have the potential to supply larger
488 volumes of fine-grained material than the bedrock made up of limestones.

489 From the clay minerals, only smectite can absorb larger amounts of water (Likos and Lu,
490 2002). However, the x-ray spectra of muscovite and smectite crystals cannot be distinguished
491 with the applied XRD method. Because the basement rocks and the Triassic schists are
492 considered to be the source of the clay minerals in the catchment area (Schlunegger et al.,
493 2009), the signal is more likely related to the fine-grained muscovite (sericite) than to the
494 smectite minerals (Scheiber et al., 2013). Therefore, swelling clay minerals are expected to
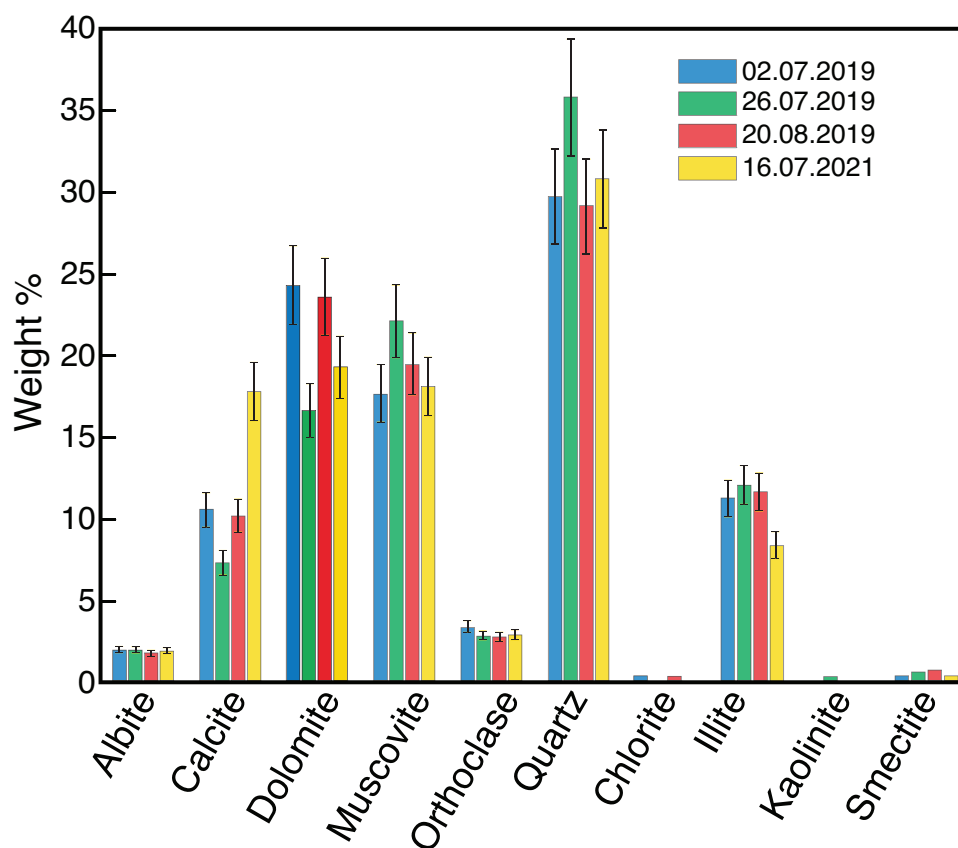495 be of minor importance in this case.

496

497 Figure 8

498 Figure 8: Mineralogic composition of four samples analyzed by powder-XRD. The black error bars indicate a
499 methodological error of 10% of the measured value. The material representing the flow on the 2nd of July 2019 was
500 exceptionally fine-grained (Table S6); the flow on the 26th of July of the same year was an event with a high velocity
501 (8.69 m/s), and it was the most rapid flow (Table 1). The debris flow on the 20th of August, again in 2019, was very
502 slow (0.89 m/s) and it was indeed the slowest flow during the survey period (Table 1). The material taken from the
503 debris flow on the 16th of July 2021 was characterized by a rather coarse-grained matrix (Table S6).

504

505 *4.5   Statistical evaluation of the debris flow properties*

506 A statistical evaluation of the debris flow parameters measured at the monitoring station shows
507 a positive correlation between velocity, flow depth, volume, and maximum discharge (Figure

508   9). While velocity, volume, and maximum discharge correlate very strongly among themselves
509   as they are physically related (auto-correlation), the correlation of these parameters with the
510   flow depth is less evident, yet a weak positive correlation is certainly visible. Accordingly, and
511   as expected (McArdell et al., 2003), a debris flow with a large volume tends to have a large
512   flow velocity and flow depth, which consequently also results in a large maximum discharge
513   and a large Froude number. On the other hand, debris flows that have a small volume are
514   also slow, and they have both a small flow depth and a low Froude number. Interestingly, clear
515   correlations between grain size, clay content and flow properties are not visible in our analyses
516   (Figure 10). Also, no correlation between the inferred water content and the volume or
517   maximum discharge was found for these events. Yet, the total friction values that are extracted
518   from the modelling results tend to show a positive correlation with the flow depth, and a weak
519   positive correlation with the density and thus a weak negative relation to the water content
520   (Figure 9).
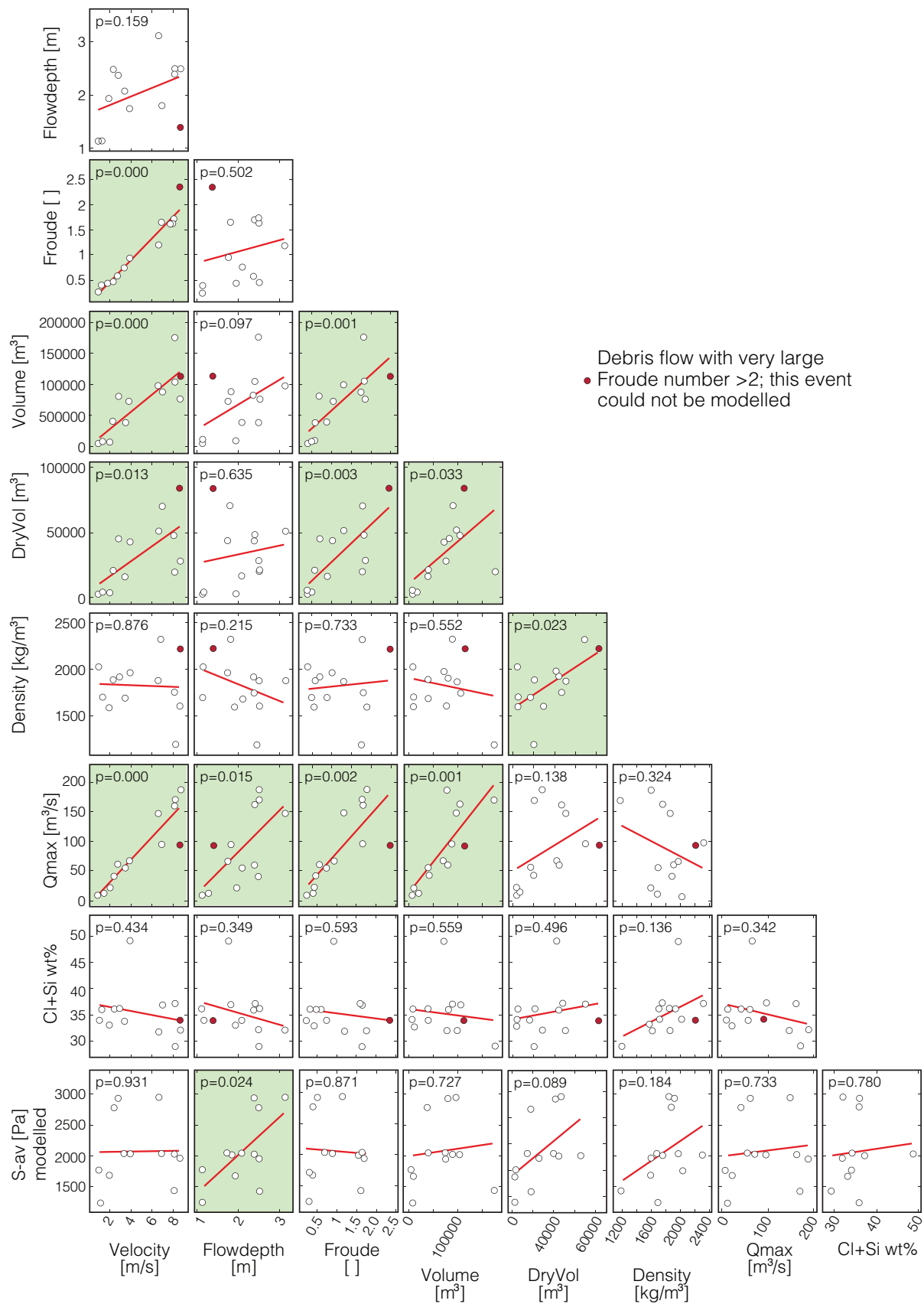
Figure 9: Statistical correlations between dynamic properties of the debris flows with a statistical p-value. For correlation tests a significance level of 0.05 is considered. Correlations with p-values < 0.05 can therefore be

considered as significant (illustrated with green color). Measurements from the monitoring station at the Illgraben and values derived from them are front velocity [m/s], maximum flow depth [m], Froude number [ ], total volume [m^3], dry sediment volume [m^3], density of a flow [kg/m^3], which points to the water content and the maximum discharge [m^3/s]. From the grain size analyses, we have the percentage of the sum of clay and silt in the sample [wt%]. From the modelling with RAMMS we get the total amount of friction [Pa] as average of all best-fit simulations of a certain event. The plots were generated using a modified version of the Correlation Matrix Scatterplot by Chow (2022) for MATLAB. Note that a statistical p-value with p = 0.000 means that the value is less than 0.0005, and therefore it is rounded down to 0.
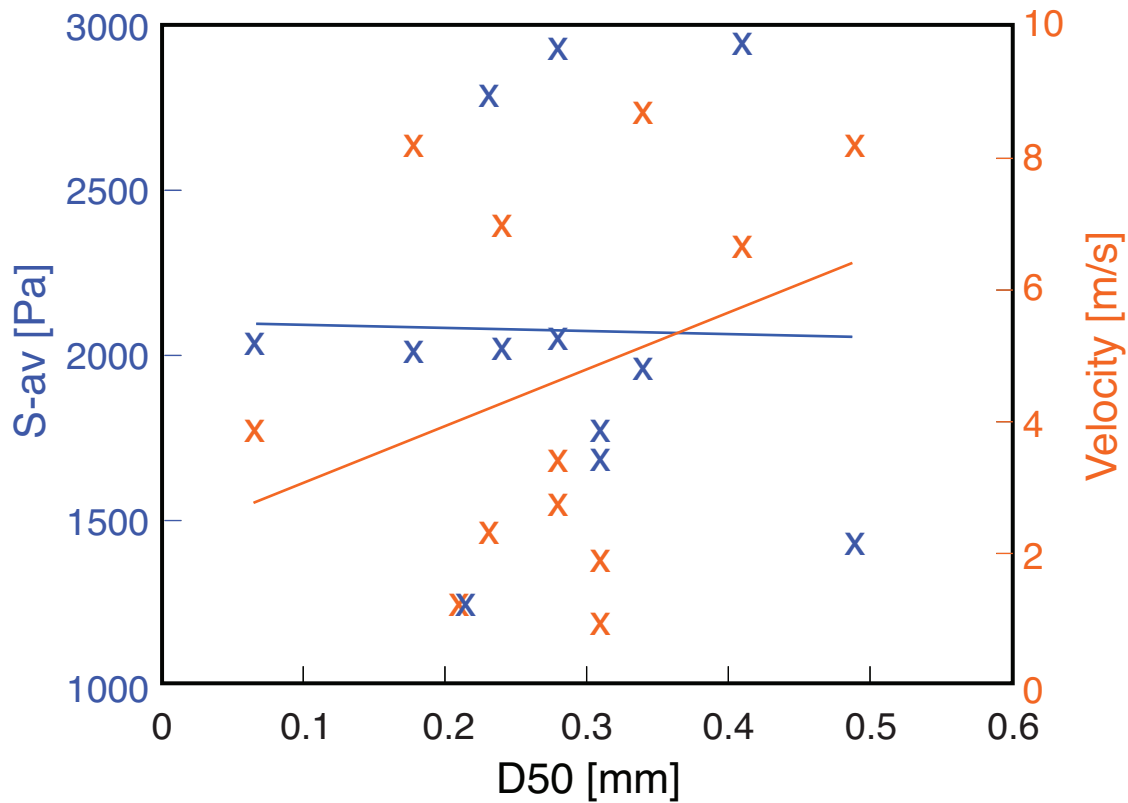
Figure 10

Figure 10: Correlation (first order polynomial trendlines accomplished by least square fitting) between the total amount of friction S-av as average of all best-fit simulations of a certain event and the D50 value of the corresponding sediment sample (blue), and correlation between the measured velocity of the flow and the D50 value of the corresponding sediment sample (red).

5   Discussion

The debris flows observed in the years 2019, 2021 and 2022 show large differences in their dynamics, where flow depths and flow velocities varied by a factor of 3 and 10, respectively. Despite these variabilities in the surveyed parameters, most of the flows could be simulated with RAMMS, and the model outputs yielded consistent results regarding the underlying controls and the simulated flow kinematics and properties (see Tables S2, S3, S4 and S5, and the related z-values). In the following section, we discuss how the various parameters such as the grain size and mineralogical distribution of the fined-grained matrix as well as the friction properties potentially exerted a control on the surveyed debris flows.

5.1   Relationships between volume, flow velocity and flow depth, and controls on friction
550   *properties*

551   The statistical tests show positive correlations between volume, flow velocity, flow depth and

552   maximum discharge rate. Our results are thus consistent with similar results reported by

553   Rickenmann (1999), de Haas et al. (2015) and Hürlimann et al. (2015) and reflect the open-

554   channel hydraulic principles used to compute these parameters (McArdell et al., 2023).

555   Indeed, as shown by the aforementioned authors, flows with larger volumes may contain a

556   larger number of pebbles and boulders, which according to Johnson et al. (2012) are likely to

557   accumulate on the front of these flows. As a result, the frictional resistance of the frontal part

558   increases (Iverson, 1997), with the consequence of a damming effect such as that the flow

559   depths will increase. We indeed see such a mechanism at work in the surveyed flows through

560   positive correlations between flow depth, flow velocity and flow volume. We thus infer that the

561   volume can be considered as the most important driving parameter for explaining the debris

562   flow dynamics in the Illgraben system and therefore can be considered as a key parameter.

563   This confirms standard practice in hazard analysis, which gives primary importance to event

564   volume. We note that this argument relies on the debris flows all having the same initial grain

565   size distribution, which, as discussed above, we can only document for sediment sizes smaller

566   than 16 mm. Yet, we acknowledge that a visual comparison of the videos (Figure S1) clearly

567   shows differences in the abundance of relatively coarse sediment (e.g., boulders). A more

568   detailed analysis on this topic will require additional data and is beyond the scope of this paper.

569   The evaluation of the RAMMS simulations shows that there are several μ–ξ pairs, which yield

570   ideal solutions upon simulating the surveyed debris flows. In particular, the same flow can

571   successfully be reproduced by RAMMS with large and low Voellmy μ–values. However, an

572   assessment of which of these possibilities is more appropriate can be found if the flow velocity

573   is used as a criterion. Indeed, our analysis showed that debris flows with a high velocity (up

574   to 6-7 m/s) tend to be dominated by a large Coulomb friction (large μ–value), whereas flows

575   with a low velocity have a low Coulomb friction (low μ–value) but a relatively high turbulent

576   friction (Figure 5). Yet for flows with velocities that are larger than 6-7 m/s, these relatively

577   simple relationships break down most likely because such flows appear to be in a condition

578   where the flow pattern is more complex (e.g., roll waves with Froude numbers that are much

579   larger than 1 to 1.5, Table 1).

580   We note that while it is tempting to interpret such low– μ flows as being 'laminar' and large– μ

581   flows as 'turbulent' (because of the low and high Froude numbers, see also Figure 5),

582   independent criteria for determining the presence or absence of turbulence in debris flows are

583   not yet available. A hydraulics-based estimate based on the Reynolds number to characterize

584   the presence or absence of turbulence (e.g. Henderson, 1966) requires estimates of the

585   rheology of the entire flow, which are not available. In addition, it is unclear to what extent

586   rheological measurements of fine sediment slurries can represent the overall viscosity of the

587   flow given the presence of other processes such as the jamming of particles in the flow

588   (Kostynic et al., 2022). Yet, such calculations are beyond the scope of this contribution.

589

590   *5.2   Influence of the grain size distribution and mineralogy*

591   The granulometric analysis of the levee deposits indicates a rather homogeneous grain size

592   distribution for the clay, silt, sand and the fine-grained gravel fraction. The grain size

593   distribution fits quite well with the granulometric analyses of the debris flow deposits at the

594   Illgraben published by Hürlimann et al. (2003). Because of a lack of correlations between the

595   relative proportion of the fine fraction to the parameters that characterize the flow properties

596   (e.g., friction and flow velocity; Figure 10), the variations in the dynamics of these flows cannot

597   be simply explained by a simple fixed friction relation such as in the Voellmy relation. This

598   inference is consistent with the notion by Iverson (2003) who states that the evolution of debris

599   flow behavior upstream of the front is likely to be complex. In the same sense, because of the

600   homogeneity of the samples with respect to the grain size distribution of the components

601   smaller than 16 mm, also the relative abundance of the sand to the fine-grained gravel fraction

602   cannot be related to variations in the flow dynamics. Nevertheless, an influence of the grain

603   size composition on the debris flow dynamics, as described by de Haas et al. (2015) and

604   Hürlimann et al. (2015), cannot be fully excluded (see section 1.1). Because the relative

605   abundances of the different fractions are similar, their potential influence on the flow properties

606   should also be similar for each event. Due to this similarity, such relationships (if present)

607   would not be detectable with the measurements presented herein. Admittedly, we also have

608   no information to exclude a potential control of the coarse-grained fraction such as coarse

609   gravel, cobbles, and boulders, on the flow dynamics, as described by de Haas et al. (2015).

610   Attempts to reconstruct the full grain size distribution are hampered by a lack of information

611   on the grain size below the surface of the flow (e.g., Uchida et al., 2021). In addition, the

612   influence of small changes of the topography on the results was not investigated here, but

613   could improve the correlations of the flow properties to grain size if adequately considered.

614   Similar to the grain size distribution of the fine-grained matrix, we do not see a relationship

615   between the mineralogical composition of the matrix and the flow properties. Among the

616   various minerals that are present in the debris flow deposits (Table S7), we expect to see a

617   control of the sheet silicates on the velocity of the flows, mainly because clay minerals and

618   particularly smectite-type of clays have the potential to absorb water in their crystal structure

619   (see section 1.1). We therefore expect that a high relative abundance of such minerals will

620   alter the flow rheology and particularly the flows' turbulent friction, which is expected to impact

621   the flow velocity. Apparently, this is not the case at the Illgraben. We consider this absence of

622   relationships to reflect a supply signal, because the relative abundance of swelling minerals

623 is negligible in the source area where other sheet silicates such as illite and muscovite crystals
624 predominate (Scheiber et al., 2013). These silicates don't have swelling properties and
625 apparently do not impact the velocity of the debris flows at the Illgraben. However, the
626 homogeneity in terms of the mineral composition and also the grain size composition between
627 the samples confirms the results of previous studies that inferred the occurrence of an efficient
628 mixing mechanism as the material is transferred from the source area to the Rhone River
629 (Schlunegger et al., 2009; Berger et al., 2011a).
630

631 **Conclusion**

632 The results obtained in the Illgraben system by comparing various debris flow parameters with
633 data from runout modelling, grain size analyses, and XRD analyses can be summarized as
634 follows:

635 1) The simulation of debris flows with RAMMS yields multiple solutions with different friction
636   coefficients μ and ξ in the Voellmy equation. The resulting Coulomb and turbulent friction
637   are correlated with the Froude number and runout velocity of the debris flow yet only as
638   long as the flow velocity is < 6-7 m/s.

639 2) The dynamics of a debris flow in the Illgraben (i.e., flow velocity and flow depth) is strongly
640   dependent on its volume. If information about the sediment volume in the source area is
641   available, the parameters for simulating a potentially worst-case debris flow and its impact
642   can theoretically be assessed with some uncertainties.

643 3) Due to the relatively large homogeneity of the deposits with respect to the grain size
644   distribution and the mineralogical composition, an efficient mixing process in the Illgraben
645   can be inferred.

646 4) Based on these data, variations in the dynamics of different debris flows cannot be
647   attributed to the grain size distributions of the clay, silt, sand or fine-grained gravel
648   fractions. Consequently, an assessment of a potential debris flow or a definition of a
649   simulation based on grain size compositions in the source area is not possible in the case
650   presented here.

651 Such relationships are particularly useful for the assessment of natural hazards, as they
652 provide specific evidence for the estimation of a debris flow and its impact.
653

659

Data availability

All data used in this paper are listed in Table 1 and in the supplementary files.

Autor contributions

BM and FS designed the study. DB conducted the experiments, collected the data and processed the samples. DB wrote the paper, with contributions by FS and BM. All authors discussed the article.

Competing interests

The authors declare that they have no conflict of interest.

References

Abraham, M.T., Satyam, N., Peddholla Reddy, S.K., and Pradhan, B.: Runout modeling and calibration of friction parameters of Kurichermala debris flow, India. Landslides, 18, 737-754. https://doi.org/10.1007/s10346-020-01540-1.

Allen, P. A.: Earth surface processes. Blackwell Science, 1997.

Badoux, A., Graf, C., Rhyner, J., Kuntner, R., and McArdell, B. W.: A debris-flow alarm system for the Alpine Illgraben catchment: Design and performance, Nat. Hazards, 49, 517–539, 2007. https://doi.org/10.1007/S11069-008-9303-X/FIGURES/7

Barshad, I.: Absorptive and swelling properties of clay-water system, Clays Clay Miner., 1(1), 70–77, 1952.

Bartelt, P., Valero, C. V., Feistl, T., Christen, M., Bühler, Y., and Buser, O.: Modelling cohesion in snow avalanche flow, J. Glaciol., 61, 837–850, 2015. https://doi.org/10.3189/2015JoG14J126

Belli, G., Walter, F., McArdell, B., Gheri, D., and Marchetti, E.: Infrasonic and Seismic Analysis of Debris-Flow Events at Illgraben (Switzerland): Relating Signal Features to Flow Parameters and to the Seismo-Acoustic Source Mechanism, J. Geophys. Res. Earth, 127, e2021JF006576, 2022. https://doi.org/10.1029/2021JF006576

Bennett, G. L., Molnar, P., McArdell, B. W., Schlunegger, F., and Burlando, P.: Patterns and controls of sediment production, transfer and yield in the Illgraben, Geomorphology, 188, 68–82, 2013. https://doi.org/10.1016/j.geomorph.2012.11.029

Berger, C., Christen, M., Speerli, J., Lauber, G., Ulrich, M., And McArdell, B. W.: A comparison of physical and computer-based debris flow modelling of a deflection structure at Illgraben, Switzerland, Data Acquisition and Modelling (Monitoring, Processes, Technologies, Models), 212–220, 2016.

695 Berger, C., McArdell, B. W., Fritschi, B., and Schlunegger, F.: A novel method for measuring

696   the timing of bed erosion during debris flows and floods, Water Res. Res., 46, 2010.

697   https://doi.org/10.1029/2009WR007993

698 Berger, C., McArdell, B. W., & Schlunegger, F.: Sediment transfer patterns at the Illgraben

699   catchment, Switzerland: Implications for the time scales of debris flow activities,

700   Geomorphology,   125,   2011a.   421–432.

701   https://doi.org/10.1016/j.geomorph.2010.10.019

702 Berger, C., McArdell, B. W., and Schlunegger, F.: Direct measurement of channel erosion by

703   debris   flows,   Illgraben,   Switzerland,   J.   Geophys.   Res.,   116,   2011b.

704   https://doi.org/10.1029/2010JF001722

705 Bumann, N.: Effect of Geological Preconditioning on Sediment Production in the Illgraben

706   Catchment [Ms thesis]. University of Bern, 2022.

707 Chatterji, P.K., and Morgestern, N.R., 1990. A modified shear strength formulation for swelling

708   clay soils. In: Proc. Symp. Physico-Chemical Aspects of Soil, Rock and Related

709   Materials, St. Louis. ASTM Spec. Tech. Publ. N1095, 118-139.

710 Choi, C. E., Ng, C. W. W., Au-Yeung, S. C. H., and Goodwin, G. R.: Froude characteristics of

711   both dense granular and water flows in flume modelling, Landslides, 12, 1197–1206,

712   2015. https://doi.org/10.1007/S10346-015-0628-8/FIGURES/11

713 Chow,   J. :   Correlation   Matrix   Scatterplot,   2022.

714   https://www.mathworks.com/matlabcentral/fileexchange/53043-correlation-matrix-

715   scatterplot

716 Christen, M., Bühler, Y., Bartelt, P., Leine, R., Glover, J., Schweizer, A., Graf, C., McArdell, B.

717   W., Gerber, W., Deubelbeiss, Y., Feistl, T., and Volkwein, A.: Integral hazard

718   management using a unified software environment numerical simulation tool "RAMMS"

719   for gravitational natural hazards, 2012. www.interpraevent.at

720 Church, M., McLean, D., and Wolcott, J.: River bed gravels : sampling and analysis, Sediment

721   Transport   in   Gravel-Bed   Rivers,   43–88,   1987.

722   https://cir.nii.ac.jp/crid/1572261549037050368.bib?lang=en

723 Coelho, A. A.: TOPAS and TOPAS-Academic: An optimization program integrating computer

724   algebra and crystallographic objects written in C++, J. Applied Crystall., 51, 210–218,

725   2018. https://doi.org/10.1107/S1600576718000183

726 de Haas, T., Braat, L., Leuven, J. R. F. W., Lokhorst, I. R., and Kleinhans, M. G.: Effects of

727   debris flow composition on runout, depositional mechanisms, and deposit morphology

728   in laboratory experiments, J. Geophys. Res. Earth Surface, 120, 1949–1972, 2015.

729   https://doi.org/10.1002/2015JF003525

de Haas, T., McArdell, B. W., Nijland, W., Åberg, A. S., Hirschberg, J., and Huguenin, P.: Flow and Bed Conditions Jointly Control Debris-Flow Erosion and Bulking. Geophys. Res. Lett., 49, e2021GL097611, 2022. https://doi.org/10.1029/2021GL097611

Deubelbeiss, Y., and Graf, C.: Two different starting conditions in numerical debris-flow models - Case study at Dorfbach, Randa (Valais, Switzerland). Jahrestagung Der Schweizerischen Geomorphologischen Gesellschaft, 2011.

Di Maio, C.: Exposure of bentonite to salt solution: osmotic and mechanical effects. Géotechnique XLVI (4), 695–707, 1996.

Di Maio, C., Santoli, L., and Schiavone, P.: Volume change behaviour of clays: the influence of mineral composition, pore fluid composition and stress state. Mechanics Mat., 36, 435-451, 2004. https://doi.org/19.1016/S0167-6636(03)00070-X

Frank, F., McArdell, B. W., Huggel, C., and Vieli, A.: The importance of entrainment and bulking on debris flow runout modeling: examples from the Swiss Alps, Nat. Hazards Earth Sys. Sci., 15, 2569-2583, 2015, https://doi.org/10.5194/nhess-15-2569-2015;

Frank, F., McArdell, B. W., Oggier, N., Baer, P., Christen, M., and Vieli, A.: Debris-flow modeling at Meretschibach and Bondasca catchments, Switzerland: sensitivity testing of field-data-based entrainment model, Nat. Hazards Earth Sys. Sci., 17, 801-815, 2017. https://doi.org/10.5194/nhess-17-801-2017

Gabus, J. H., Weidmann, M., Sartori, M., and Burri M.: Blatt 1287 Sierrre - Geologischer Atlas der Schweiz 1:25 000, Erläuterungen, Bundesamt für Landestopografie swisstopo, 2008.

Henderson, F.M.: Open Channel flow. New York, MacMililan, 1966.

Hirschberg, J., Badoux, A., McArdell, B. W., Leonarduzzi, E., and Molnar, P.: Evaluating methods for debris-flow prediction based on rainfall in an Alpine catchment, Nat. Hazards Earth Sys. Sci., 21, 2773–2789, 2021. https://doi.org/10.5194/NHESS-21-2773-2021

Hirschberg, J., Fatichi, S., Bennett, G. L., McArdell, B. W., Peleg, N., Lane, S. N., Schlunegger, F., and Molnar, P.: Climate Change Impacts on Sediment Yield and Debris-Flow Activity in an Alpine Catchment, J. Geophys. Res. Earth Surface, 126, e2020JF005739, 2021. https://doi.org/10.1029/2020JF005739

Hirschberg, J., McArdell, B. W., Badoux, A., and Molnar, P.: Analysis of rainfall and runoff for debris flows at the Illgraben catchment, Switzerland. Debris-Flow Hazards Mitigation: Mechanics, Monitoring, Modeling, and Assessment - Proceedings of the 7th International Conference on Debris-Flow Hazards Mitigation, 693–700, 2019.

Hübl, J., Suda, J., Proske, D., Kaitna, R., and Scheidl, C.: Debris Flow Impact Estimation, International Symposium on Water Management and Hydraulic Engineering, 137–148, 2009. https://www.researchgate.net/publication/258550978

767 Hürlimann, M., McArdell, B. W., and Rickli, C.: Field and laboratory analysis of the runout
768   characteristics of hillslope debris flows in Switzerland, Geomorphology, 232, 20–32,
769   2015. https://doi.org/10.1016/J.GEOMORPH.2014.11.030

770 Hürlimann, M., Rickenmann, D., and Graf, C.: Field and monitoring data of debris-flow events
771   in the Swiss Alps, Can. Geotech. J., 40, 161–175, 2003. https://doi.org/10.1139/t02-087

772 Iverson, R. M.: The physics of debris flows, Rev. Geophys., 35, 245–296, 1997.
773   https://doi.org/10.1029/97RG00426

774 Jianjun, Z., Zhang, Y.X.: Numerical simulation of debris flow runout using Ramms: a case
775   study of Luzhuang Gully in China. Computer modeling in Engineering & Science, 121,
776   981-1009. https://doi.org/10.32604/cmes.2019.07337.

777 Johnson, C. G., Kokelaar, B. P., Iverson, R. M., Logan, M., Lahusen, R. G., and Gray, J. M.
778   N. T.: Grain-size segregation and levee formation in geophysical mass flows, J.
779   Geophys. Res. Earth Surface, 117, 2012. https://doi.org/10.1029/2011JF002185

780 Kaitna, R., Palucis, M. C., Yohannes, B., Hill, K. M., and Dietrich, W. E.: Effects of coarse
781   grain size distribution and fine particle content on pore fluid pressure and shear behavior
782   in experimental debris flows, J. Geophys. Res. Earth Surf., 121, 415–441,2016.
783   doi:10.1002/2015JF003725.

784 Likos, W. J., and Lu, N.: Water vapor sorption behavior of smectite-kaolinite mixtures. Clays
785   Clay   Mineral,   50,   553–561,   2002.
786   https://doi.org/10.1346/000986002320679297/METRICS

787 McArdell, B. W., Bartelt, P., and Kowalski, J.: Field observations of basal forces and fluid pore
788   pressure   in   a   debris   flow,   Geophys.   Res.   Lett.,   34,   2007.
789   https://doi.org/10.1029/2006GL029183

790 McArdell, B. W., and Sartori, M.: The Illgraben torrent system. In E. Reynard (Ed.), World
791   geomorphological landscapes, Landscapes and landforms of Switzerland (pp. 367-378),
792   2021. https://doi.org/10.1007/978-3-030-43203-4_25.

793 McArdell, B. W.: Field measurements of forces in debris flows at the Illgraben: implications for
794   channel-bed   erosion.   Int.   J.   Erosion   Control   Eng.,   9,   194-198,   2016.
795   https://doi.org/10.13101/ijece.9.194

796 McArdell, B. W., Hirschberg, J., Graf, C., Boss, S., and Badoux, A.: Illgraben debris-flow
797   characteristics 2019-2022. EnviDat. 2023. https://www.doi.org/10.16904/envidat.378.

798 Medina, V., Hürlimann, M. and Bateman, A.: Application of FLATModel, a 2D finite volume
799   code, to debris flows in the northeastern part of the Iberian Peninsula. Landslides 5,
800   127–142, 2008. https://doi.org/10.1007/s10346-007-0102-3

801 Mikoš, M., and Bezak, N.: Debris flow modelling using RAMMS model in the Alpine
802   environment with focus on the model parameters and main characteristics. Front. Earth
803   Sci., 8 – 2020, 2021. https//doi.org/10.3389/feart.2020.605061.

Naef, D., Rickenmann, D., Rutschmann, P., and McArdell, B. W.: Comparison of flow resistance relations for debris flows using a one-dimensional finite element simulation model, Nat. Hazards Earth Sys. Sci., 6, 155–165, 2006. www.nat-hazards-earth-syst-sci.net/6/155/2006/

Pierson, T. C.: Flow behavior of channelized debris flows, Mount St. Helens, Washington. In A. Abrahams (Ed.), Hillslope Processes (pp. 269–296), 1986.

Rickenmann, D.: Empirical Relationships for Debris Flows, Nat. Hazards, 19, 47–77, 1999.

Rietveld, H. M.: A profile refinement method for nuclear and magnetic structures, J. Applied Crystallography 2, 65–71, 1969. https://doi.org/10.1107/S0021889869006558

Salm, B.: Flow, flow transition and runout distances of flowing avalanches, Annal. Glaciol. 18, 221–226, 1993. https://doi.org/10.3189/S0260305500011551

Salm, B., Burkard, A., and Gubler, H. U.: Berechnung von Fliesslawinen. Eine Anleitung fuer Praktiker mit Beispielen, In Mitteilungen des Eidg. Institutes für Schnee- und Lawinenforschung (Vol. 47), 1990.

Scheiber, T., Pfiffner, O.A., and Schreurs, G.: Upper crustal deformation in continent-continent collision: A case study from the Bernhard nappe complex (Valais, Switzerland). Tectonics, 32, 1320-1342, 2013. https://doi.org/10.1002/tect.20080.

Schlunegger, F., Badoux, A., McArdell, B. W., Gwerder, C., Schnydrig, D., Rieke-Zapp, D., and Molnar, P.: Limits of sediment transfer in an alpine debris-flow catchment, Illgraben, Switzerland, Quat. Sci. Rev., 28, 1097–1105, 2009. https://doi.org/10.1016/j.quascirev.2008.10.025

Schlunegger, F., Garefalakis, P.: Einführung in die Sedimentologie. Schweizerbart, Stuttgart, 305 p., 2023.

Schürch, P., Densmore, A. L., Rosser, N. J., and McArdell, B. W.: Dynamic controls on erosion and deposition on debris-flow fans, Geology, 39, 827–830, 2011. https://doi.org/10.1130/G32103.1

Simoni, A., Mammoliti, M., and Graf, C.: Performance Of 2D debris flow simulation model RAMMS. Ann. Int. conf. GEOS, 2012. https://doi.org/10.5176/2251-3361_GEOS12.59

Swisstopo: Bundesamt für Landestopografie, 2022. https://www.swisstopo.admin.ch/de/geodata.html

Uchida, T., Nishiguchi, Y., McArdell, B. W., and Satofuka, Y.: The role of the phase shift of fine particles on debris flow behavior: a numerical simulation for a debris flow in Illgraben, Switzerland, Can. Geotech. J., 58, 23-34, 2021. https://doi.org/10.1139/cgj-2019-0452

Voellmy, A.: Über die Zerstörungskraft von Lawinen, Schweiz. Bauzeitschrift, 73, 212–217, 1995. https://doi.org/10.5169/seals-61891

840   WSL.   RAMMS::DEBRISFLOW   User   Manual   v1.8.0   (v1.8.0).   WSL,   2022.
841   https://ramms.slf.ch/en/modules/debrisflow.html
842
843